GSJ: Volume 13, Issue 6, June 2025, Online: ISSN 2320-9186

www.globalscientificjournal.com

Analyzing The Influence Of Defects On The Mechanical Properties Of Microcomposite Aircraft Structures

Kabasha Kizito[1], Semayat Fanta[2]

[1]M-Tech Student, Aerospace Engineering Department, EDU, Bishoftu, Ethiopia
(E-mail: kabashak@yahoo.com).

[2]Phd, Aerospace Engineering Department, EDU, Bishoftu, Ethiopia
(E-mail: semayat.iitk2016@gmail.com)

Abstract - *Microcomposites are increasingly utilized in the aerospace industry due to their superior mechanical and thermal properties, including a high strength-to-weight ratio, enhanced fatigue resistance, and thermal stability. Despite these advantages, the presence of manufacturing and in-service defects—such as voids, fiber misalignment, delamination, and microcracks—can significantly compromise the structural integrity and performance of composite components. These defects can lead to reduced tensile and compressive strength, early fatigue crack initiation, diminished fracture toughness, and premature failure under operational stresses. This research systematically investigates the effects of such defects on the mechanical behavior of microcomposite structures, with a primary focus on aerospace applications. A combined methodology involving analytical evaluation, and numerical simulations—specifically Finite Element Analysis (FEA) using ABAQUS—was employed. At the microscale level, two Representative Volume Elements (RVEs) of unidirectional (UD) carbon/epoxy composites, each measuring (1 × 1 × 1) mm, were modeled: one non-voided and one voided (2.6%) with both spherical and irregularly shaped voids randomly distributed within the matrix. The simulations assessed stress distribution, deformation patterns, and failure mechanisms under four distinct loading conditions: longitudinal tensile (along fiber direction, Z-axis), transverse tensile (X-axis), transverse compression (Y-axis), and in-plane shear (XY-plane). The results revealed a significant reduction in mechanical properties for the voided RVEs across all loading cases. Both Young's modulus and effective strength decreased, with the most pronounced deterioration observed in the transverse direction—approximately 15% reduction in effective strength and 4.5% in Young's modulus. To enhance the reliability, performance, and longevity of aerospace composite components and ensure optimal material behavior under operational loads, it is recommended to minimize voids during manufacturing by optimizing processing parameters and implement robust quality control systems for void detection using non-destructive evaluation techniques. These measures will contribute to the development of more durable, lightweight, and fuel-efficient aerospace structures.*

Keywords: Microcomposite, Graphite-Epoxy Composite, Micromechanical properties, Representative volume element, Finite element analysis, Effective strength

1. INTRODUCTION

The use of advanced composites in aerospace structures has grown significantly, driven by a demand for materials that are lighter, stronger, and more resilient than traditional metals. Among these materials, microcomposites are subgroup of composite materials featuring reinforcements on a micron scale—offer significant weight-to-strength advantages critical for efficient aircraft design. These materials are often composed of polymer matrices embedded with carbon fibers, glass fibers, or particles such as graphene, which enhance mechanical properties like stiffness, tensile strength, and fatigue resistance. However, their performance can be highly sensitive to manufacturing defects that compromise structural integrity and safety, especially in demanding aerospace environments[1].

For example, microcomposite structures are commonly used in components like fuselages, wing panels, and control surfaces, where lightweight properties and high mechanical strength are essential. But small imperfections such as voids, fiber misalignments, or microcracks can lead to stress concentrations, reducing tensile and compressive strength and making the material more susceptible to fatigue and failure over time. Defects like voids or delaminations are particularly problematic in high-stress areas, as they act as sites for crack initiation and propagation, potentially leading to catastrophic failures in critical flight situations[2].

Various non-destructive evaluation (NDE) methods, such as ultrasonic inspection, X-ray computed tomography (XCT), and digital image correlation, are used to detect and analyze defects in microcomposites. These techniques help determine the effects of defects on properties such as stiffness, fatigue resistance, and fracture toughness. For instance, XCT imaging provides a 3D visualization of internal voids and inclusions, enabling engineers to quantify defect sizes and distributions within a structure, as seen in Figure 1 (an example XCT image illustrating voids in a fiber-reinforced microcomposite panel).
In one case study, defects in carbon fiber-reinforced microcomposites used in aircraft wings were found to reduce their load-bearing capacity by up to 25% under repeated loading conditions. Similarly, matrix cracking in the microcomposite landing gear structures can propagate rapidly, leading to delamination and eventual structural failure under heavy impact during landing. Such studies underscore the importance of understanding defect behavior and devising methods to mitigate their effects to enhance safety and durability[3].

The demand for more resilient microcomposites necessitates continued research to understand the influence of defects on mechanical performance fully. This thesis investigates how different defect types, including voids, inclusions, and fiber misalignments, impact the overall structural integrity of microcomposite materials in aerospace applications.

The historical development of microcomposites in aerospace applications highlights significant advancements in material science and engineering aimed at enhancing aircraft performance. Microcomposites, primarily involving polymer matrices reinforced with fibers or particles, evolved from early composite materials, which were first used in aerospace structures in the 1960s. Initially, composites such as fiber-reinforced plastics offered considerable weight savings over metals but faced challenges in mechanical reliability, as the influence of defects on these properties was not yet well-understood [1].

By the 1970s and 1980s, advancements in manufacturing techniques and fiber-reinforcement technology allowed composites to replace traditional materials like aluminum in various structural components, notably in military aircraft. This period also saw the introduction of carbon-fiber-reinforced polymers (CFRPs), which offered improved strength-to-weight ratios. However, early studies on CFRPs highlighted significant issues with void formation, fiber misalignment, and delamination, which posed risks to structural integrity under operational loads [2]. This led to increased interest in understanding how manufacturing defects and in-service damage could compromise material properties, spurring further research into defect analysis.

Modern microcomposites, particularly those incorporating nanotechnology and advanced reinforcement materials like carbon nanotubes and graphene, have shown promise in achieving even higher strength and durability. However, their increased complexity has also introduced new challenges in defect management, as smaller-scale defects can propagate and significantly affect mechanical performance. Advanced analytical tools such as X-ray computed tomography (XCT) and progressive failure analysis (PFA) emerged as critical for identifying and simulating defect impacts at micro and nano scales [1].

The need to understand and mitigate the effects of defects has grown as microcomposites are used more extensively in commercial aircraft, where they are critical for safety and performance. Research continues to focus on developing predictive modeling techniques and manufacturing processes that minimize defects, contributing to safer, more efficient aircraft. This historical background reflects the field's evolution from rudimentary composites to sophisticated microcomposites and highlights the ongoing importance of defect analysis for ensuring material reliability in aerospace applications.

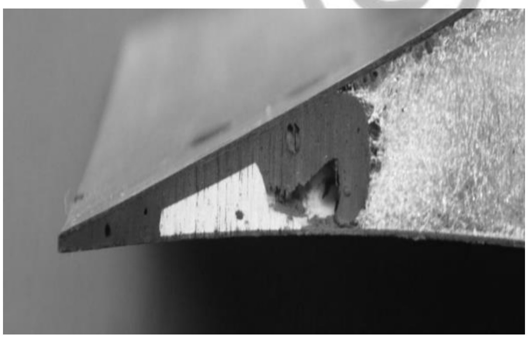

Figure 1: Voids in resin filler [5]

Polymer microcomposites are increasingly used in the aerospace industry due to their lightweight, high strength, and enhanced performance properties. Here are several examples of aircraft parts made from polymer microcomposite structures:

Fuselage Sections: Microcomposites are used in fuselage construction to reduce weight while maintaining structural integrity. These materials improve strength-to-weight ratio, enhance fatigue resistance, and offer better damage tolerance than traditional materials.

Wing Components: Certain parts of the wing, including wing skins and ribs, are made from polymer Microcompositescto enhance stiffness, reduce weight, and improve fuel efficiency.

Engine Nacelles: Engine nacelles, which house aircraft engines, benefit from Microcomposites due to their heat resistance, lightweight properties, and ability to withstand aerodynamic forces.

Radomes: Radomes, which protect radar systems on aircraft, are often made from polymer microcomposites because of their excellent electromagnetic transparency, impact resistance, and lightweight structure.

Interior Panels: Microcomposites are used for interior cabin panels and components like overhead bins, sidewalls, and floor panels to reduce weight while maintaining structural performance and improving fire resistance.

Tail Sections: Horizontal and vertical stabilizers, along with other tail components, can be constructed using microcomposite materials for improved aerodynamics and structural efficiency.

Landing Gear Doors: Microcomposites are used in the landing gear doors to reduce weight and improve impact resistance, helping to absorb the stresses during takeoff and landing cycles.

Control Surfaces (Ailerons, Elevators, Rudders): Microcomposites are incorporated into control surfaces to enhance mechanical properties such as stiffness and durability while reducing the weight of moving parts.

Fan Blades and Engine Components: In some advanced aircraft engines, Microcomposites are used for fan blades and other components due to their high temperature tolerance, strength, and fatigue resistance.

Fairings: Microcomposites fairings, which streamline airflow around joints or protrusions, provide weight reduction and enhanced durability against weather conditions [6].

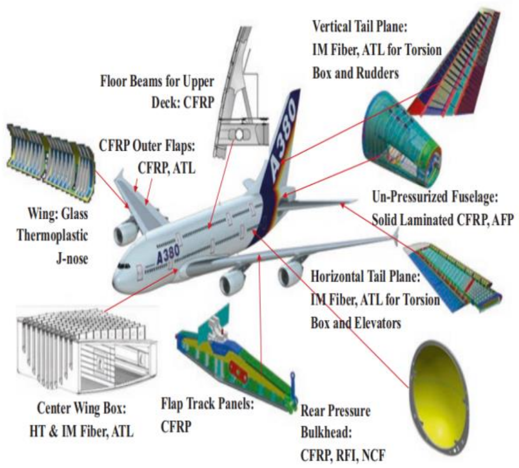

Figure 2: The material distribution of the Airbus A380 airplane[6].

Materials Used in the Construction of Aircraft Parts

Carbon Fibre-Reinforced Polymers are probably the most important class of composite materials utilized in the aircraft business. Carbon fibre is viewed as fibres with a content of at least 90 % carbon. The term graphitic fibre is utilized to portray fibres with a content of close to 100% carbon. Today, carbon fibre is the dominant fibre in the advanced composite materials industry.

In the last two decades, the properties of carbon strands have increased spectacularly as a consequence of the demand for more grounded and lighter materials, especially from the aerospace business. As a solidarity-to-weight ratio, carbon fibre is the best material that can be delivered on an industrial scale on any occasion. Carbon fibres are more expensive than glass fibres but offer a better combination of good strength, light weight, and high modulus values. The breaking strength of carbon fibre is equal to that of glass, while its modulus is three to four times that of glass [48].

The materials used in the Airbus A380's body design are displayed in Figure 2. More than half of modern aircraft, including the Boeing 787 Dreamliner, are composed of carbon fibre composites [49]. Every generation of Boeing aircraft has seen a rise in the percentage of composite materials used, with the largest being the 50% of composite materials used in the next 787 Dreamliner [49]. As with the 787 Dreamliner, the weight of the composite elements of the aircraft is reduced by about 20%. In the early 1980s, Airbus also used composites in primary architectural structures [10]. The company created the first carbon Sustainability 2024, 16, 46324 of 23 fibre fall beam for a large commercial air conditioner, the A340, in the late 1990s; composite materials are used throughout the new A380 [49].

A new conductive composite material was required to address the increased risks associated with the air conditioner, such as lightning strikes and ice accumulation, which resulted in a significant decline in its performance. Presently, air conditioners are manufactured using composite materials that do not lead power well, leaving them vulnerable to repeated destruction by weather [49]. Following the discovery and development of nanoscale fortifications, graphene, carbon nanotubes (CNTs), and nanofibres are now regarded as essential elements of next-generation built-up composites [49]. Without the need for extra fillers, the mechanical support and other important characteristics like electrical and thermal conductivity can be enhanced by including these nano-fortifications in polymer metrics. Therefore, these problems will be resolved when these conductive materials are used in the aviation industry [49].

Table1: showing common Defects existing in Aerospace industry

S/N	TYPE OF DEFECT	LIKELY CAUSE	DETECTION METHOD	EFFECTS	MITIGATION
1	**VOID**	1. Dissolved air within the resin 2. Air stirred into the resin	- X-ray computed tomography (XCT)	Voids reduce the effective cross-sectional area available for load-	ultrasonic inspection and in-process thermography helps to minimize void formation by allowing quick adjustments to ma

		3. Trapped air in a filament bundle 4. Residual solvent carrier 5. Reaction products from the curing process 6. Volatilization of low-molecular-weight components of the resin		bearing, leading to localized stress concentrations, which degrade properties like tensile strength, fracture toughness, and fatigue resistance	nufacturing parameters
2.	**Fiber wrinkle and waviness defects of composites**	excessive compaction, or uneven resin flow -mishandling	- Shearography and ultrasonic C-scans	A misaligned fiber disrupts the composite's ability to uniformly distribute load along its length	- Use automated fiber placement (AFP) - Ensure precise control over the layup process to avoid uneven fiber placement - Conduct regular inspections of raw materials
3	**Delamination and Matrix Cracking**	- inadequate bonding between plies - unchecked tinny cracks tiny cracks within the resin matrix	- ultrasonic phased-array technology, -thermography - even laser shearography	- weakens the material's load-bearing capability	- Enhanced Interlaminar Toughness - Optimized Design and Loading Conditions
4	**Resin-Rich and Resin-Starved Areas**	poor impregnation control during layup	Ultrasonic inspection and XCT	-Resin-rich areas are prone to cracking under mechanical stress - Disruption of the structural homogeneity of the aerocomposite structures	consistence resin application, monitoring impregnation pressure, and using automated layup methods help maintain uniform resin distribution
5	**Inclusions and Foreign Particles**	often introduced during the manufacturing process through dust, metal particles	Ultrasonic inspection and X-ray computed tomography (XCT)	- reducing overall strength, elasticity, and fatigue resistance, especially under dynamic loading conditions -crack initiation point	- stringent cleanroom protocols, -filtered environments, - advanced sealing of machinery.
6	**Interfacial Weakness**	Insurficient bonding between fiber and matrix often due to insufficient adhesion between fiber and resin	Nanoscale observation techniques, such as scanning electron microscopy (SEM) and atomic force microscopy (AFM)	- inadequate load transfer from the matrix to the fibers - reduced tensile strength, elasticity, and impact resistance	-Improved resin formulations, -optimized curing cycles, and - use of surface treatments or coupling agents

2. MATERIALS AND METHODS

1.1 Materials

Graphite carbon fibers, also known as carbon fibers, are strong, lightweight filaments used in aerospace to make aircraft bodies and jet engine parts. They are made from thin strands of carbon that are woven into fabrics and combined with a plastic resin to create composite materials. **Epoxy resin** is a thermosetting resin that's used as a matrix in the aerospace industry to make aircraft structures, propulsion systems, and more. Epoxy resin is a common choice because it's lightweight, strong, and durable.

Evaluation of the Four Elastic Moduli

There are four elastic moduli of a unidirectional lamina [42]:

- Longitudinal Young's modulus, *E*1
- Transverse Young's modulus, *E*2
- Major Poisson's ratio, ν12
- In-plane shear modulus, *G*12

2.7.1 Strength of Materials Approach

From a unidirectional lamina, take a representative volume element that consists of the fiber surrounded by the matrix (Figure 19). This representative volume element (RVE) can be further represented as rectangular blocks. The fiber, matrix, and the composite are assumed to be of the same width, h, but of thicknesses tf, tm, and tc, respectively. The area of the fiber is given by [42]

$A_f = t_f h$

(2.1)

The area of the matrix is given by

$A_m = t_m h$

(2.2)

and the area of the composite is given by

$A_c = t_c h$

(2.3)

The two areas are chosen in the proportion of their volume fractions so that the fiber volume fraction is defined as [42]

$$Vf = \frac{A_f}{A_c} = \frac{t_f}{t_c} \quad (2.4)$$

and the matrix fiber volume fraction *Vm* is

$$V_m = \frac{A_m}{A_c};= \frac{t_m}{t_c};=1-V_f$$

(2.5)

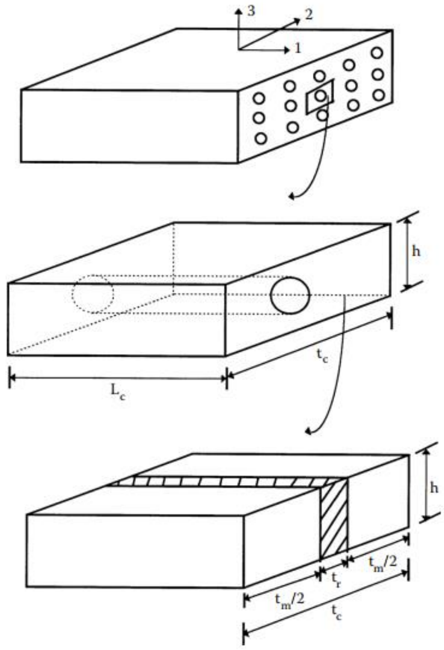

Figure 3: Representative element of Unidirectional Lamina [42]

Therefore, using the above equations, it is observed that [42]

Assumptions in Analytical Calculations of Elastic Moduli (E_1, E_2, G_{12})

Longitudinal Modulus (E_1) – Rule of Mixtures:

- The fibers and matrix are perfectly bonded, meaning there is no inter-facial debonding.
- The composite behaves as a homogeneous material in the longitudinal direction.
- Fibers carry most of the load in the longitudinal direction due to their high stiffness.
- The matrix only provides load transfer but does not significantly contribute to stiffness.
- The strain is uniform across the fiber and matrix (iso-strain assumption).

$$E_1 = E_f V_f + E_m V_m \quad (2.6)$$

Transverse Modulus (E_2) – Inverse Rule of Mixtures:

- The fibers and matrix experience the same transverse stress (iso-stress assumption).
- The composite behaves as a layered system, with the matrix playing a larger role in stiffness.
- Fibers are assumed to be evenly distributed within the matrix.
- The transverse modulus is computed based on a series model, assuming uniform fiber distribution.
- Perfect fiber-matrix bonding is assumed, meaning no interfacial failure.

$$\frac{1}{E_2} = \frac{V_f}{E_f} + \frac{V_m}{E_m}$$
(2.7)

Semi-Empirical Models

The most useful of these models include those of Halphin and Tsai because they can be used over a wide range of elastic properties and fiber volume fractions. [42]

$$\frac{E_2}{E_m} = \frac{1+\varepsilon\eta V_f}{1-\eta V_f}, \eta = \frac{(E_f / E_m)-1}{(E_f / E_m)+\varepsilon} \quad (2.71)$$

The term Ɛ is called the reinforcing factor and depends on the following:
• Fiber geometry
• Packing geometry
• Loading conditions
For example, for a fiber geometry of circular fibers in a packing geometry of a square array, Ɛ = 2. For a rectangular fiber crosssection of length a and width b in a hexagonal array, Ɛ = 2(a/b), where b is in the direction of loading.

$$\nu_{12} = \nu_f V_f + \nu_m V_m \quad (2.8)$$

Shear Modulus (G_{12}) – Halpin-Tsai or Semi-Empirical Relations:

- Fibers and matrix are assumed to be perfectly bonded and act together in shear deformation.
- The composite's response in shear is influenced by both fiber and matrix shear stiffness.
- A semi-empirical correction factor (such as Halpin-Tsai) is often introduced to fit experimental data.
- Shear stress is assumed to be uniformly distributed in the matrix and fiber.
- The fiber cross-section remains circular, and deformation follows linear elastic behavior [51].

$$\frac{1}{G_{12}} = \frac{V_f}{G_f} + \frac{V_f}{G_m}$$
(2.9)

2.8 Evaluation of Ultimate Strengths

I. Longitudinal Tensile Strength [41]
Assume that
• Fiber and matrix are isotropic, homogeneous, and linearly elastic until failure.

Now, if
(σf)ult = ultimate tensile strength of fiber,
Ef = Young's modulus of fiber,
(σm)ult = ultimate tensile strength of matrix,
Em = Young's modulus of matrix,

$$(\sigma_1^T)_{ult} = (\sigma_f)_{ult} V_f + (\varepsilon_f)_{ult} E_m (V_m)$$
(2.10)

II. Transverse Tensile Strength [41]
Assume that,
• A perfect fiber–matrix bond
• Uniform spacing of fibers
• The fiber and matrix follow Hooke's law
• There are no residual stresses

$$(\sigma_2^T) = \sigma_m \left(\frac{1}{V_m}\right)$$, also $$(\sigma_2^T)_{ult} = E_2 (\varepsilon_2^T)_{ult} \quad (2.11)$$

Where
$$(\varepsilon_2^T)_{ult} = \left[\frac{d}{s}\frac{E_m}{E_f} + \left(1 - \frac{d}{s}\right)\right](\varepsilon_m^T)_{ult}$$
(2.12)

s = distance between center of fibers
d = diameter of fibers

In-Plane Shear Strength

Assume that one is applying a shear stress of magnitude τ12, and then that the shearing deformation in the representative element is given by the sum of the deformations in the fiber and matrix [41],

$$(\tau_{12})_{ult} = G_{12}(\gamma_{12})_{ult} \tag{2.13}$$

3.5 Void Content

During the manufacture of a composite, voids are introduced in the composite as shown in Figure 3.2. This causes the theoretical density of the composite to be higher than the actual density. Also, the void content of a composite is detrimental to its mechanical properties. These detriments include lower

- Shear stiffness and strength
- Compressive strengths
- Transverse tensile strengths
- Fatigue resistance
- Moisture resistance

A decrease of 2 to 10% in the preceding matrix-dominated properties generally takes place with every 1% increase in the void content [41] For composites with a certain volume of voids V*v* the volume fraction of voids V*v* is defined as

$$V_\upsilon = \frac{\upsilon_\upsilon}{\upsilon_c}$$

(3)

Then, the total volume of a composite (vc) with voids is given by

$$\upsilon_c = \upsilon_f + \upsilon_m + \upsilon_\upsilon$$

(3.1)

By definition of the experimental density ρ_{ce} of a composite, the actual volume of the composite is

$$\upsilon_c = \frac{w_c}{\rho_{ce}}$$

(3.2)

and, by the definition of the theoretical density ρct of the composite, the theoretical volume of the composite is

$$\upsilon_f + \upsilon_m = \frac{w_c}{\rho_{tc}}$$

(3.3)

Then, substituting the preceding expressions (19) and (20) in Equation (21),

$$\frac{w_c}{\rho_{ce}} = \frac{w_c}{\rho_{ct}} + \upsilon_\upsilon$$

(3.4)

The volume of void is given by

$$\upsilon_\upsilon = \frac{w_c}{\rho_{ce}}\left(\frac{\rho_{tc} - \rho_{ce}}{\rho_{tc}}\right) \tag{3.5}$$

Substituting Equation (20) and Equation (21) in Equation (22), the volume fraction of the voids is

$$V_\upsilon = \frac{\upsilon_\upsilon}{\upsilon_c} = \frac{\rho_{tc} - \rho_{ce}}{\rho_{tc}} \tag{3.6}$$

2.7.2 Void characteristics on the mechanical response of unidirectional composites

The prediction of the mechanical properties of UD composites has been a long-standing problem for many researches. Various micromechanical models have been proposed to evaluate the elastic properties of UD composites based on Eshelby's tensor, such as the Halpin–Tsai model, the Chamis model and the generalized self-consistent model.

These micromechanical models can directly give analytical expressions of elastic properties, in which some of them also study the influence of voids on mechanical properties. Christensen modeled the voids as circular cylindrical inclusions inherent in the generalized self-consistent method. It was found that the effective modulus is insensitive to the matrix Poisson's ratio υ_m over the range of $0 \leq \upsilon_m < 1$ and it is only in the range of negative values of υ_m that strong sensitivity to υ_m emerges. Ge et al. (2020) proposed a modified Chamis model to calculate elastic properties of UD composites with void defects, which can be expressed by [36]

$$E_1 = V_f E_{f1} + (1 - V_f) E_m (1 - V_{m\upsilon})^2$$

(2.10)

$$E_2 = E_{=} \frac{E_m (1 - V_{m\upsilon})^2}{1 - \sqrt{V_f}[1 - E_m (1 - V_{m\upsilon})^2 / E_{f2}]}$$

(2.11)

$$G_{12} = G_{13} = \frac{E_m(1-V_{m\upsilon})^2}{2(1+\upsilon_m) - \sqrt{V_f}[2(1+\upsilon_m) - E_m(1-V_{m\upsilon})^2 / G_{f23}]}$$
(2.12)

$$\upsilon_{12} = \upsilon_{13} = V_f \upsilon_{f12} + V_m \upsilon_m$$
(2.13)

where $V_{\upsilon m}$(= V_υ/V_m) is defined as the volume fraction of voids in equivalent matrix, V_i (i = f,m.υ) is the volume fraction of constituent, Em is the elastic modulus of matrix, E1 , E2 , G12 and G23 are the longitudinal, transverse, longitudinal shear and transverse shear modulus of fiber respectively, υ12 is the longitudinal Poisson's ratio of fiber [36].

As for strength, Chamis proposed an empirical formula to calculate the matrix strength in the case of spherical voids, which can be written as:

$$X^I_{m\upsilon}(S_{m\upsilon}) = [1 - \sqrt{\frac{4V\upsilon}{(1-V_f)\pi}}]X^I_m(S_{m\upsilon}); I \in \{t,c\} \quad (2.14)$$

where X^I_m (I ∈ {t,c}) represents the tensile strength and compressive strength of matrix, $X^I_{m\upsilon}$ denotes the strength considering voids, it is the same for shear strength. Then, the following equations considering void defects can be applied to predict the strength properties of UD composites [36]:

$$X^l_1 = V_f X^l_f$$
$$X^t_2 = \left[1 - \left(\sqrt{V_f} - V_f\right)\left(1 - \frac{E_m}{E_{f2}}\right)\right] X^t_{mv}$$
$$S_{12} = \left[1 - \left(\sqrt{V_f} - V_f\right)\left(1 - \frac{G_m}{G_{f12}}\right)\right] S_{mv}$$
(2.15)

where X^I_t, X^1_2 and S_{12}(23) are longitudinal, transverse and shear strength of UD composites respectively. Considering the possible failure modes under longitudinal compression, the strengths for fiber fracture, shear failure and micro buckling are given by [36] equations below

$$X^{c1}_1 = V_f X_c \quad (2.16)$$

Thus, the longitudinal compression strength of UD composites is predicted by [36]

$$X^c_l = \frac{1}{3}\left(X^{c1}_l + X^{c2}_l + X^{c3}_l\right)$$
(2.18)

2.1 Assumptions in Numerical Analysis (e.g., Finite Element Analysis - FEA in Abaqus) [51]

- **Heterogeneous Material Modeling:** The composite is modeled explicitly with individual fiber and matrix domains instead of a homogenized approach.
- **Interfacial Bonding Consideration:** The numerical model can include different fiber-matrix interface conditions, such as perfect bonding or interfacial debonding.
- **Stress/Strain Distribution:** Unlike analytical methods, numerical analysis accounts for non-uniform stress and strain distribution within the RVE.
- **Geometrical Effects:** The actual arrangement of fibers (square, hexagonal, or random) affects the results. In contrast, analytical models assume an idealized fiber arrangement.
- **Boundary Conditions Influence:** The applied boundary conditions (e.g., periodic, symmetry, displacement-based) can impact the computed moduli.
- **Voids and Defects:** Numerical methods can incorporate voids, defects, and irregularities, which are usually ignored in analytical calculations.
- **Nonlinear Material Properties:** While analytical methods generally assume linear elastic behavior, numerical models can incorporate nonlinear plasticity for both the matrix and fibers.
- **Shear Lag Effects:** The stress transfer between fibers and the matrix is captured more accurately than in analytical models.

MORI-TANAKA'S TENSOR

Mori-Tanaka theory, a micromechanical model, predicts the effective elastic properties of composite materials, including the transverse modulus, by considering the stress and strain distribution within the composite's constituents. It's particularly effective for materials with anisotropic matrix properties.

In 1973, Mori-Tanaka proposed a rational approach to correlate averaged stresses and strains of the constituent fiber with those of the matrix in a composite. Later in 1987, Benveniste[2] found that the Mori-Tanaka's approach can be reformulated by making use of the equivalent inclusion idea in terms of a more compacted tensor, which is called the Mori-Tanaka's tensor here and in the following. This tensor in a way only depends on an Eshelby's tensor[3]. From this tensor, all of the effective elastic properties of the UD composite can be determined.

Thus far, the Eshelby-Mori-Tanaka'smethod has become very popular in the composite community. Moreover, a lot of work has been done to study mechanical behaviors of hybrid composites containing various kinds of inclusion shapes, including ellipsoidal family with different aspect ratios, from penny-shaped disc, spherical inclusion, to non-circular cylinder reinforcement, and non-ellipsoidal fillers . Different inclusion configurations in addition to uniform alignment have also been taken into account, such as randomly dispersed orientations.

According to Mori-Tanaka's theory

$$E_2 = E_m\left[\frac{1+AV_f}{1-BV_f}\right], where A = \frac{E_f/E_m - 1}{1+\frac{E_f}{E_m}.\frac{1-\mu_m}{\mu_m}}, B = \frac{1-\mu_m}{\mu_m + \frac{E_f}{E_m}(1-\mu_m)} \qquad (3.61)$$

Where μ_m is the Matrix Poisson's ratio
Now considering the Void content, E_2'=
$E_2^{'} = E_2(1-V_v)$, where V_v= Void volume fraction [54].

Materials: Carbon Fiber Reinforced

Table 1: Carbon Fiber Reinforced parameters

s/n	Properties	Value	Units
Reinforcement(Carbon Fiber/ Graphite)			
1	Volume Fraction	0.63	
2	Poission's Ratio. U12	0.3	
3	Young's Modulus, E11	230	Gpa
4	Young's Modulus, E22	22	Gpa
5	Shear Modulus,G12	22	Gpa
6	Axial tensile strength	2067	Mpa
7	length	1000	MicroMetre
8	Radius	150	MicroMetre
9	Density	1780	Kg/m3

Epoxy Matrix Composite

Table 2: Epoxy Matrix Composite parameters

s/n	Properties	Value	Units

Epoxy			
1	Volume Fraction of matrix (non voided)	0.37	
2	Volume fraction of matrix (voided)	0.34	
3	Volume fraction of void	0.2666	
4	Poission's Ratio. υ	0.3	
5	Young's Modulus, E11	3.4	Gpa
6	Young's Modulus, E22	3.4	Gpa
7	Shear Modulus,G12	1.308	Gpa
8	Axial tensile strength	72	Mpa
9	length	1000	MicroMetre
10	height	1000	MicroMetre
11	Density	1200	Kg/m3

Geometry Modeling

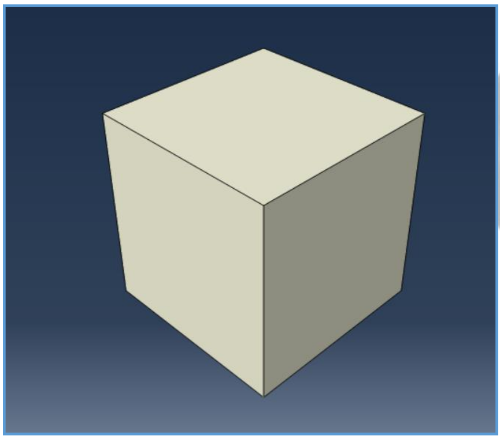

(a)

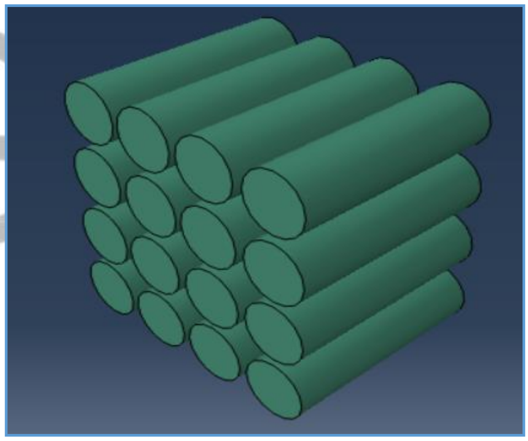

(b)

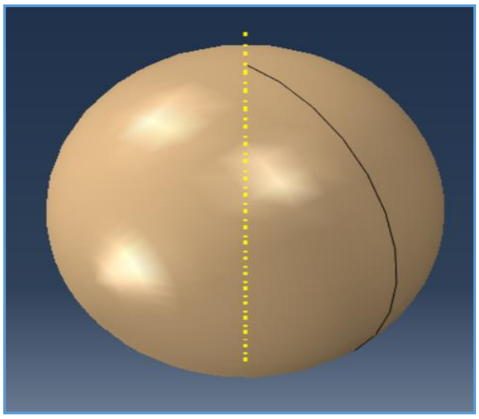

(c)

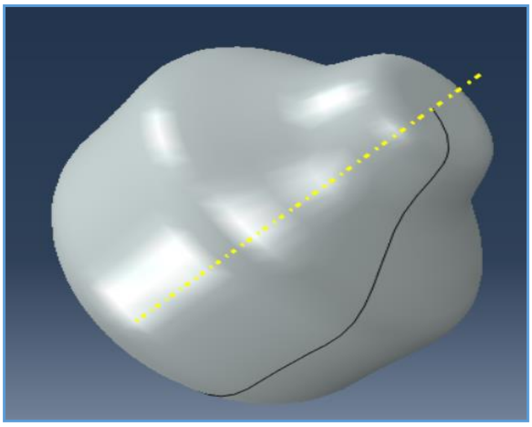

(d)

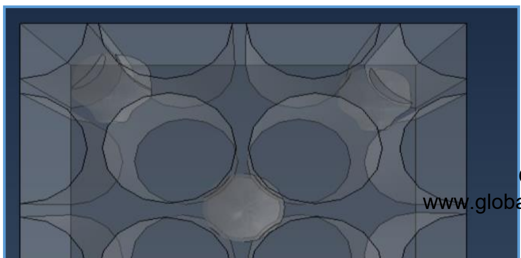

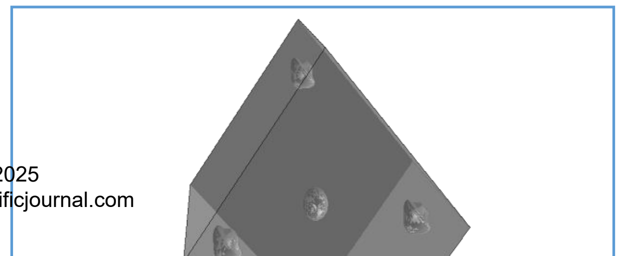

Gjkk

(e) (f)

igure 4: Geometries (a)Matrix (b)Fibre (c)spherical void (d)shapeless void (e) UD composite (f) Porous Media

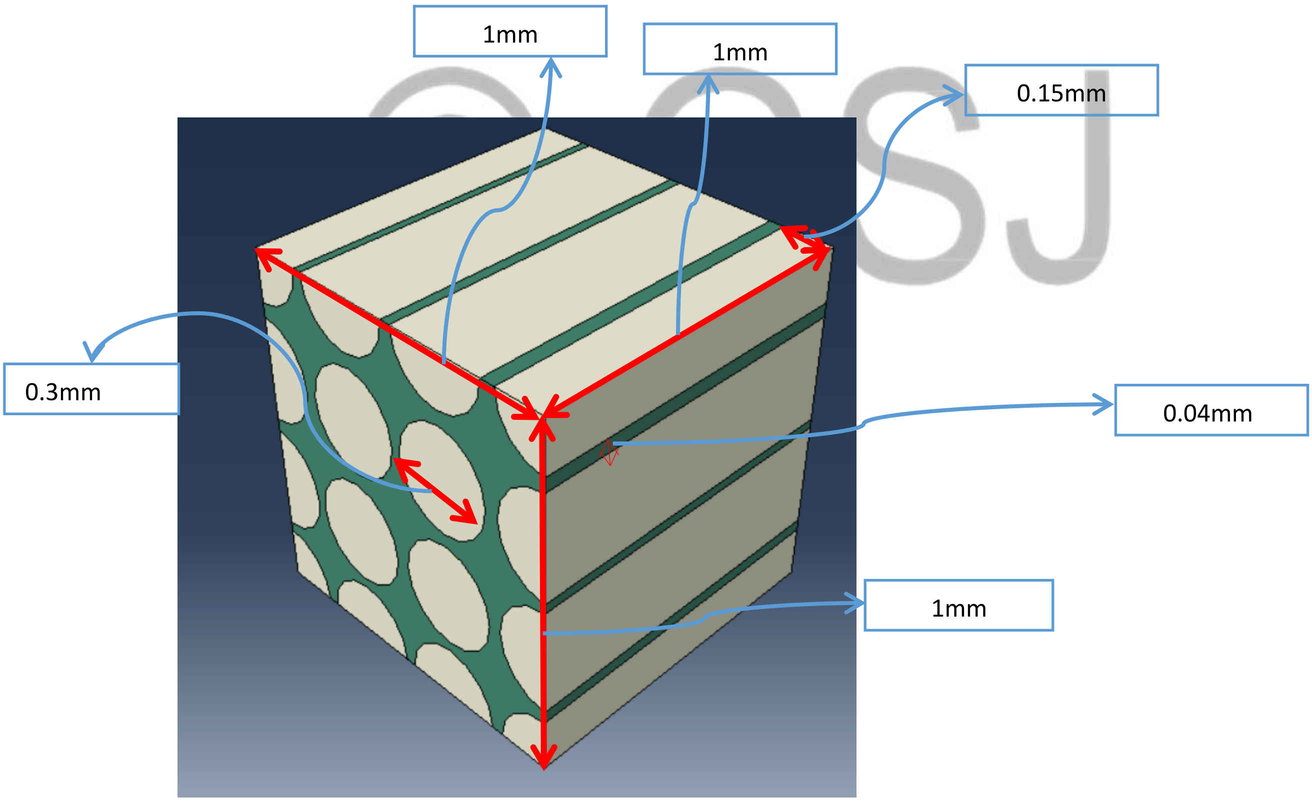

Figure 5: CFRP dimensions

Mesh generation

Mesh generation: A highly-quality computational mesh of the RVE was generated, ensuring the appropriate resolution and capture of stress-strain distributions of all grip points accurately. As mesh size decreases from **0.09**

mm to **0.042 mm**, the computed force increases and gradually stabilizes.Convergence is clearly observed at **0.045 mm to 0.042 mm**, indicating the solution has become mesh-independent with 0.6% error.

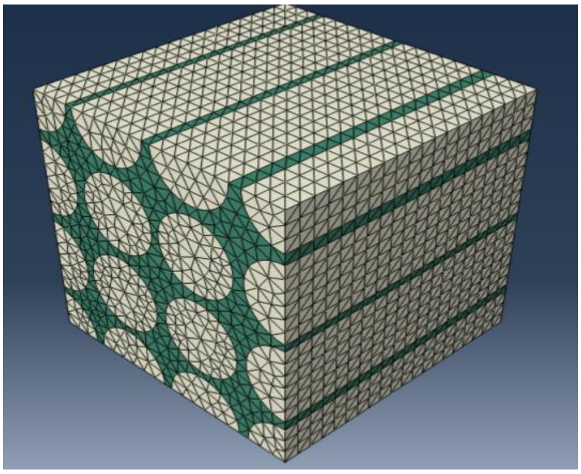

Figure 6: Meshing , problem size

Numerical analysis using Abaqus Cae software

This finite element analysis the model was conducted in four cases in each of the two models of Non-voided and Voided CFRP composites.

Non-Voided Geometry FEA

CASE I: Tensile deformation along fibre axis (Z-axis).

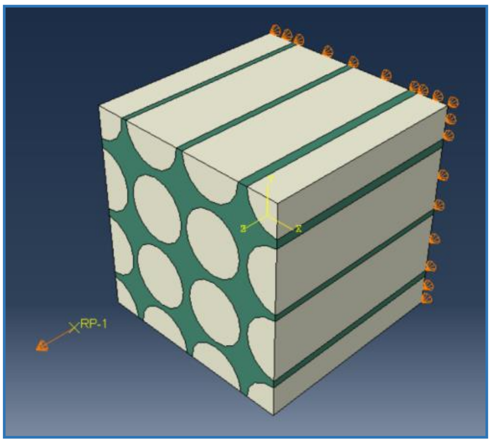

(a)

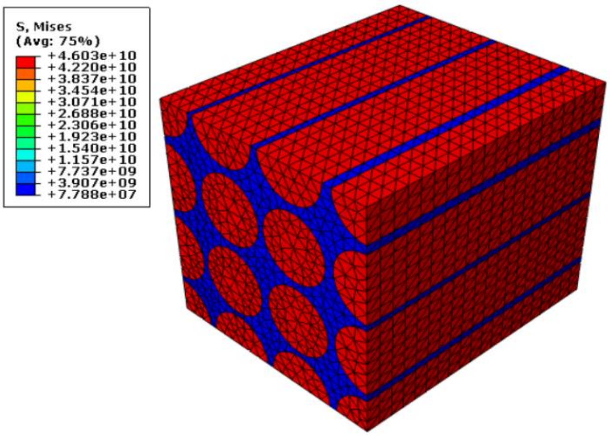

(b)

Figure 7:(a) loading condition for case I (b) tensile deformation of the model

CASE II: Compression deformation transverse to fibre axis (Y-axis).

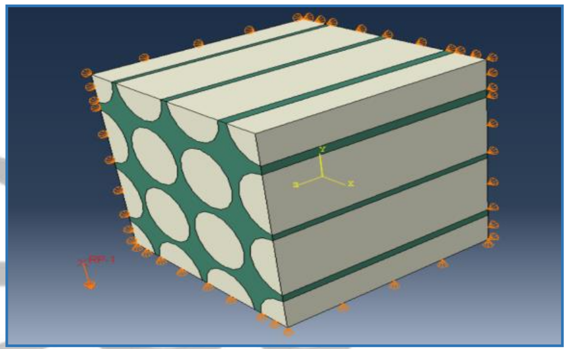

(a)

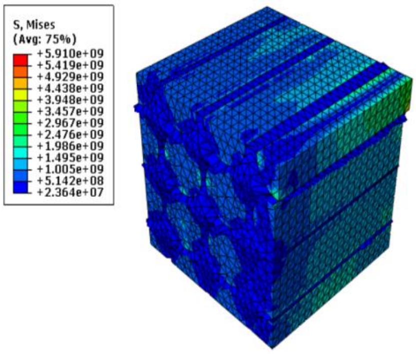

(b)

Figure 8: compression deformation (a)Loading condition and (b) model after compressionin Y drection

CASE III: Shear deformation on XY plane.

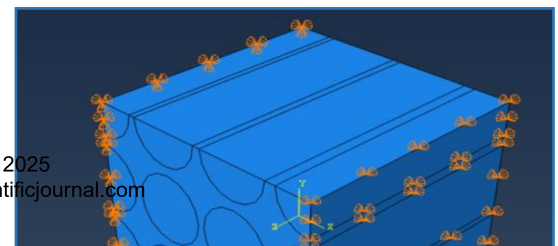

(a)

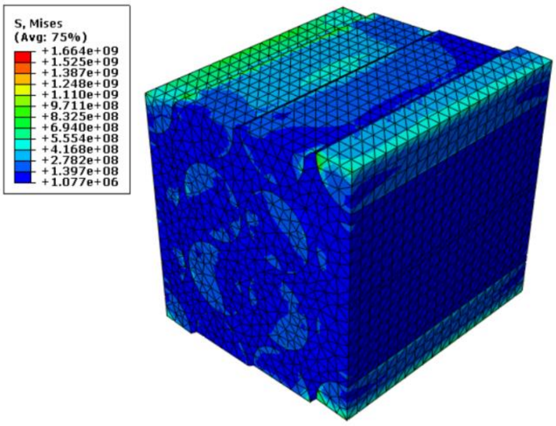

(b)

Figure 9: shear deformation

CASE IV: Tensile deformation in x-axis

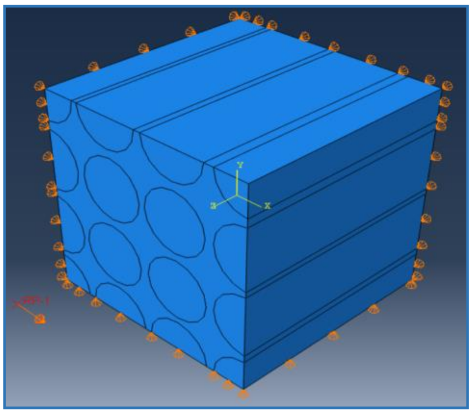

(a)

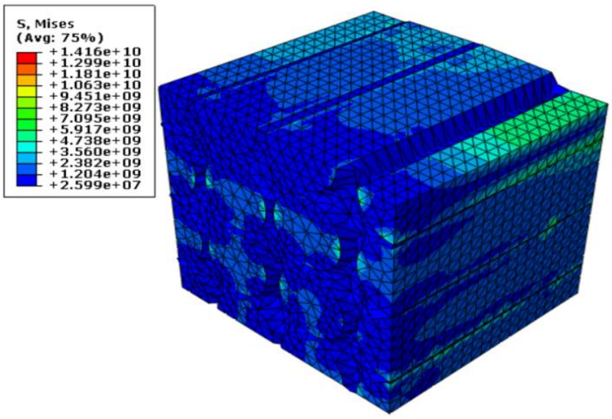

(b)

Figure 10; Tensile deformation in x-axis for a nonvoided UDcomposite structure, (a) Boundary condition (b) Deformation

Voided Geometry FEA

CASE I: Tensile deformation along fibre axis (Z-axis).

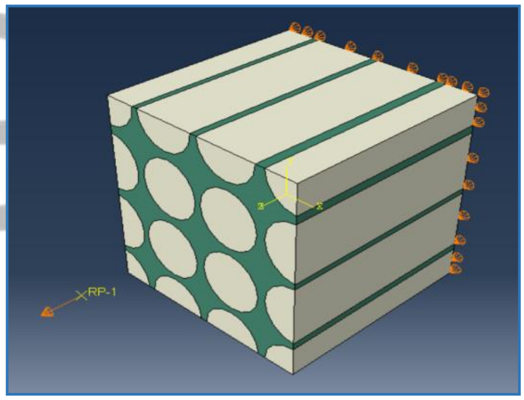

(a)

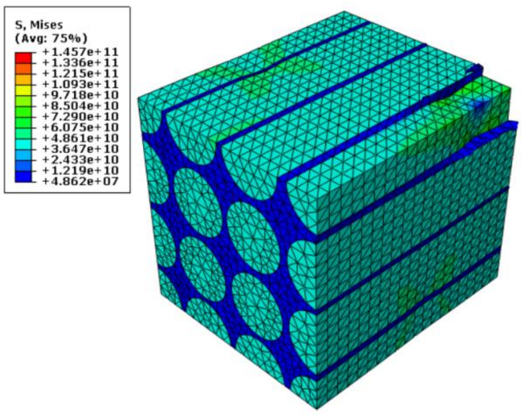

(b)

Figure 11: voided model , (a) loading condition for case I (b) tensile deformation of the model

CASE II: Compression deformation transverse to fibre axis (Y-axis).

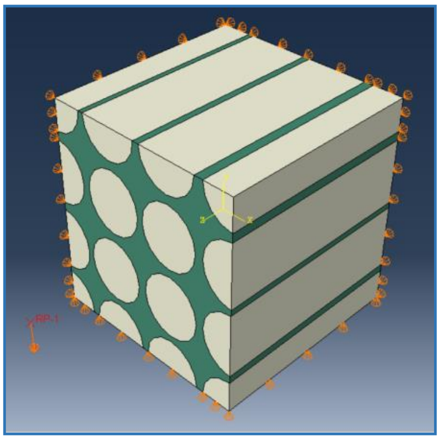

(a)

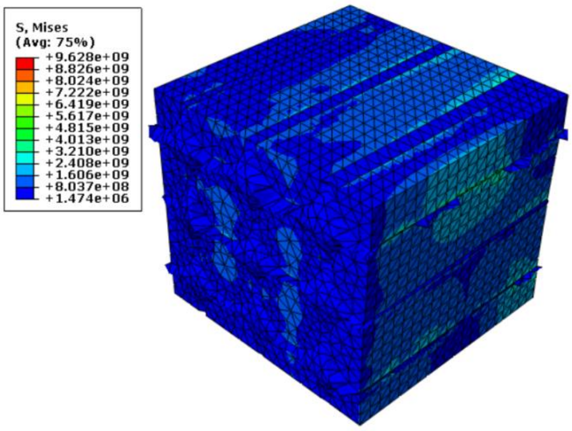

(b)

Figure 12: compression deformation (a)Loading condition and (b) model after compressionin Y drection.

CASE III: Shear deformation on XY plane for a voided model

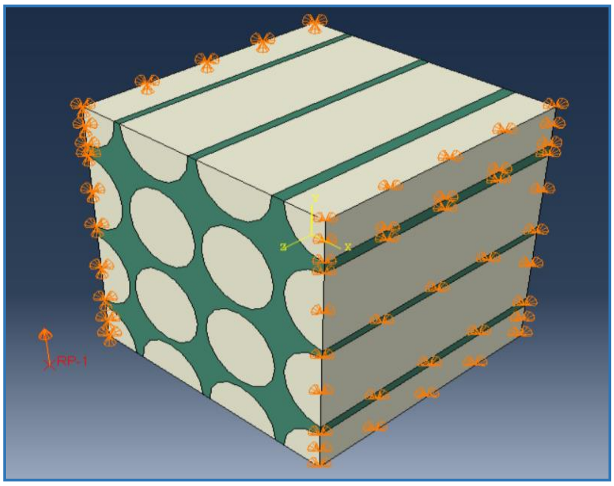

(a)

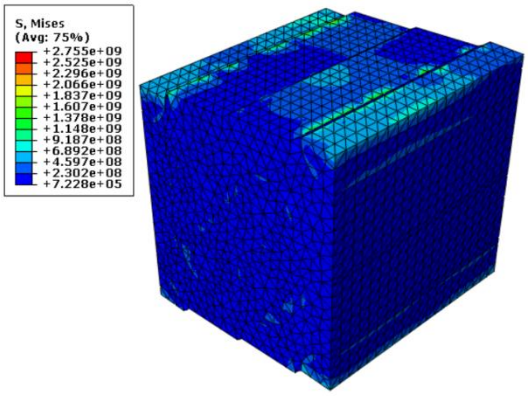

(b)

Figure 13: shear deformation for a voided model

CASE IV: Tensile deformation in x-axis voided udcomposite structure

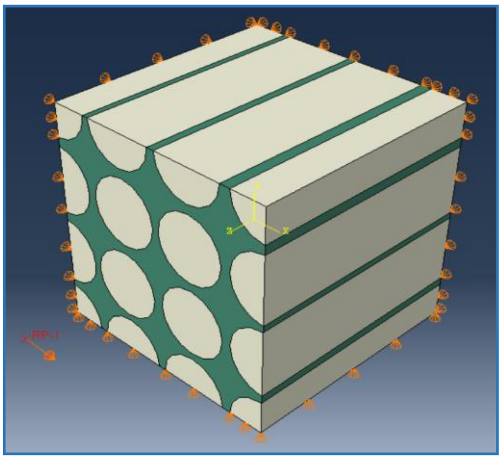

(a)

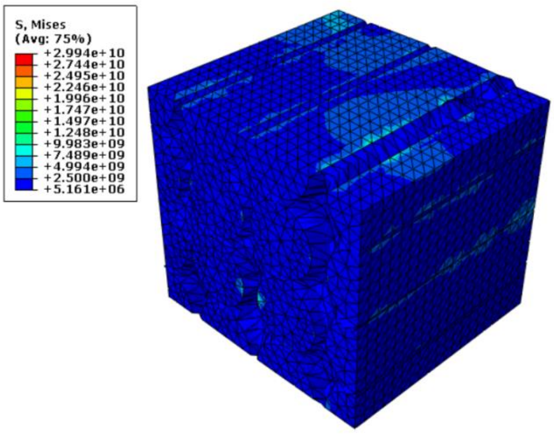

(b)

Figure 14: Tensile deformation in x-axis for a voided UDcomposite structure, (a) Boundary condition (b) Deformation

RESULT AND DISCUSSION

This chapter presents the results obtained from the numerical simulations of Microcomposite Representative Volume Elements (RVE) (1x1x1)mm as seen in figure 25 with and without voids. The mechanical behavior was assessed for four loading cases:
(i) tensile loading in the fiber direction (z-axis).
(ii) compressive loading in the y-axis (transverse to fiber direction),
(iii) shear loading in the xt-plane
(iv) Tensile deformation in x-axis
The impact of voids on the mechanical properties was analyzed by comparing voided and non-voided RVEs.

4.1 Tensile Response in Z-Axis (Fibre direction)

Tensile Loading Along the Fiber Direction (Z-Axis):

The tensile behavior along the fiber direction was assessed to understand fiber-dominated mechanical performance. The results indicate that voids have a relatively lower impact compared to the transverse direction, as the fiber reinforcement still carries the majority of the load. However, reductions in modulus and strength are still observed due to weaker matrix support.

Key Findings:
I. Tensile modulus in fiber direction is less affected by voids compared to transverse loading.
II. Failure strain remains relatively stable, though stress at failure reduces by 1.36% in voided cases.
III. Voids lead to minor reductions in load transfer efficiency between fibers and matrix.
IV. Fibre Breakage (at High Void Content) – While the fibers primarily bear the load, excessive voids can lead to stress concentrations that initiate premature fiber fractures, especially under extreme tensile loads.

V. Matrix Cracking, Debonding at the Fibre-Matrix Interface, Microvoid Coalescence Leading to Macrocracks.

Table 3: Tensile Loading Along the Fiber Direction (a) for non voided structure and (b) for voided structure.

RVE Type used	NonVoidedUD	
Length of RVE	1000	µm
Width of RVE	1000	µm
Height of RVE	1000	µm
Young's Modulus	146.356	Gpa
Effective Strength	29300.00	Mpa

(a)

RVE Type used	VoidedUD	
Length of RVE	1000	µm
Width of RVE	1000	µm
Height of RVE	1000	µm
Young's Modulus	144.658	Gpa
Effective Strength	28900	Mpa

(b)

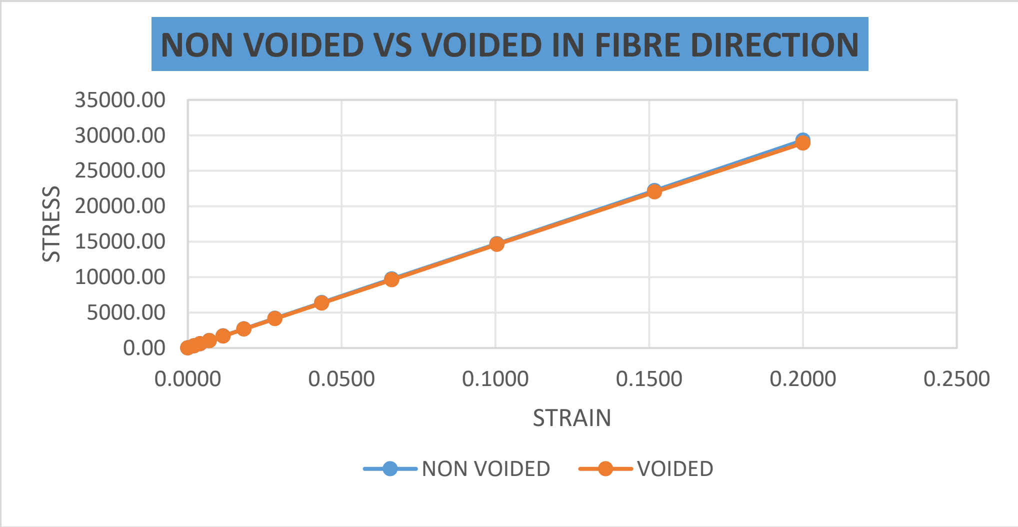

Figure 15: Tensile loading in Fibre direcrion (Z-axis)

4.2 Tensile Response in X-Axis (Transverse to Fiber Direction)

The tensile behavior of the composite in the x-axis was examined to evaluate its resistance to deformation perpendicular to the fiber orientation. The stress-strain curves for both voided and non-voided configurations indicate that the presence of voids significantly reduces the tensile strength and stiffness. The reduction in modulus and ultimate strength in the voided structure can be attributed to stress concentrations around the voids, which initiate early failure see table 4.4.

Table 4: Tensile Response in X-Axis (Transverse to Fiber Direction)(a) for non voided structure and (b) for voided structure.

RVE Type used	Non-voidedUD	
Length of RVE	1000	µm
Width of RVE	1000	µm
Height of RVE	1000	µm
Young's Modulus	17.13	Gpa
Effective Strength	648.0	Mpa

(a)

RVE Type used	VoidedUD	
Length of RVE	1000	µm
Width of RVE	1000	µm
Height of RVE	1000	µm
Young's Modulus	16.35	Gpa
Effective Strength	550	Mpa

(b)

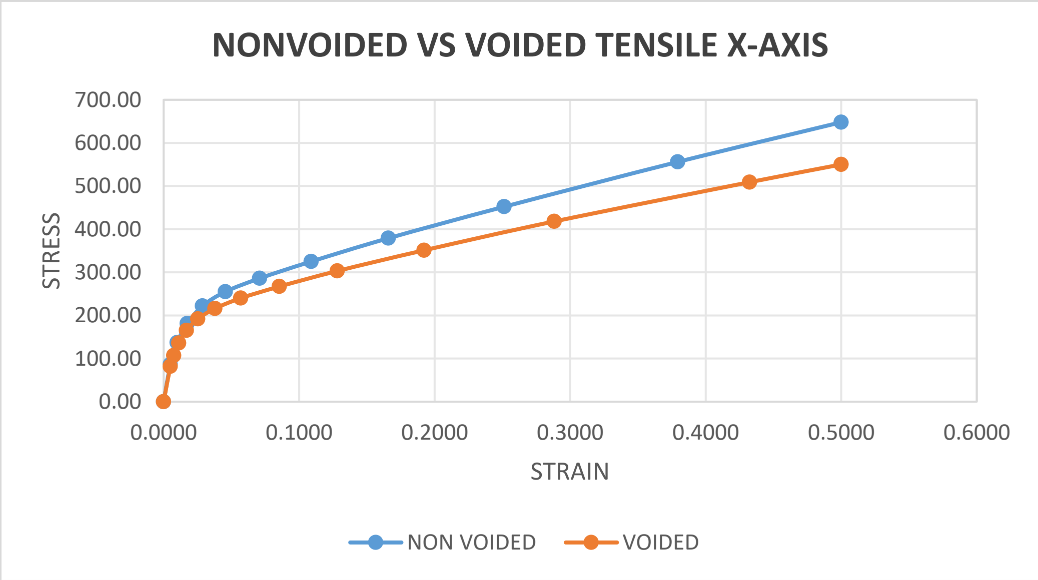

Figure 16: tensile loading in Transverse direction (X-axis)

Key Findings:

I. The non-voided RVE exhibits higher stiffness and failure stress compared to the voided RVE.

II. Voids introduce localized stress concentrations, accelerating failure initiation.

III. The reduction in effective tensile strength is quantified at 15% compared to the non-voided case.

IV. Matrix Cracking – Since transverse tensile loading relies heavily on the matrix for load bearing, voids act as stress concentrators, leading to premature matrix cracking.

4.3 Compression Response in Y-Axis (Transverse to Fiber Direction)

The compressive behavior in the transverse direction was analyzed to assess the failure mechanisms under crushing loads. The stress-strain curves demonstrate that voids significantly affect the compressive strength, leading to premature failure due to micro-buckling and localized collapse.

Table 5: Compression responses in Y-Axis(Transverse to Fiber Direction)(a) for non voided structure and (b) for voided structure.

RVE Type used	Non-voidedUD	
Length of RVE	1000	µm
Width of RVE	1000	mm
Height of RVE	1000	mm
Young's Modulus	18.0	Gpa
Effective Strength	420.0	Mpa

(a)

RVE Type used	voidedUD	
Length of RVE	1000	mm
Width of RVE	1000	mm
Height of RVE	1000	mm
Young's Modulus	17.28	Gpa
Effective Strength	367.74	Mpa

(b)

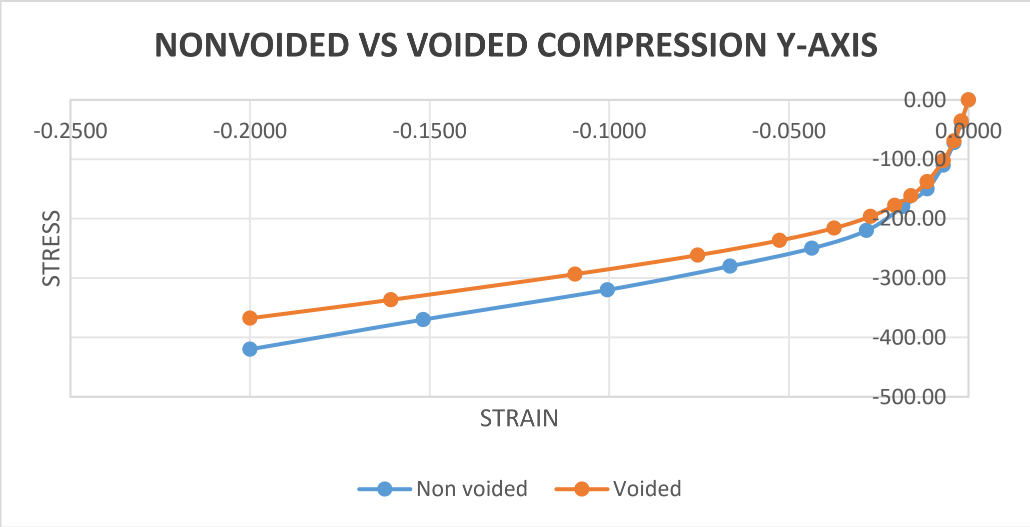

Figure 17: Compression responses in Y-Axis(Transverse to Fiber Direction

Key Findings:

I. Compressive modulus and strength are lower in voided RVEs compared to non-voided ones.

II. Voids lead to non-uniform stress distribution, promoting early buckling.
III. The reduction in effective tensile strength is quantified at 12.44% compared to the non-voided case.

IV. Failure strain in voided specimens is significantly lower due to reduced load-bearing capability.

4.4 Shear Response in XT-Plane

The shear response was evaluated in the XT-plane to determine the influence of voids on interlaminar shear strength. The voided RVE exhibits lower shear stiffness and ultimate strength due to weaker matrix-fiber interactions and increased stress concentrations.

Table 6: Shear response in XY plane (a) for non voided structure and (b) for voided structure.

RVE Type used	Non-voidedUD	
Length of RVE	1000	µm
Width of RVE	1000	µm
Height of RVE	1000	µm
Young's Modulus	3.238	Gpa
Effective Strength	49.89	Mpa

(a)

RVE Type used	VoidedUD	
Length of RVE	1000	µm
Width of RVE	1000	µm
Height of RVE	1000	µm
Young's Modulus	3.01	Gpa
Effective Strength	46.20	Mpa

(b)

Key Findings:

GSJ: Volume 13, Issue 6, June 2025
ISSN 2320-9186

I. Shear stiffness decreases in voided samples by 6.8% and the effective strength decreased by 7.4%.

II. Ultimate shear strength is affected by void distribution and orientation.

III. The presence of voids enhances crack initiation along the fiber-matrix interface.

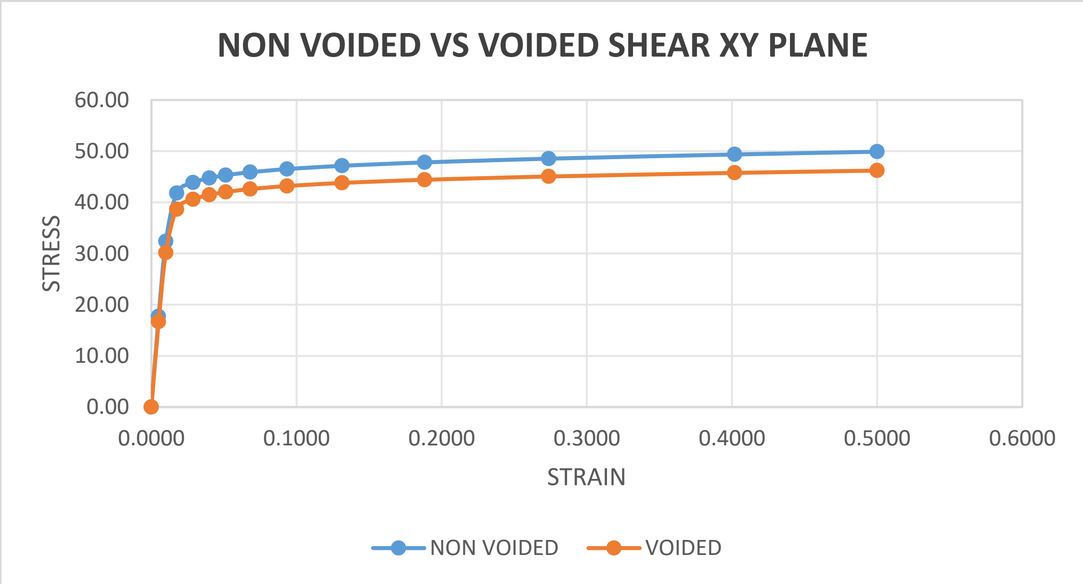

Figure 18: Shear response in XY plane

Comparative Analysis of Voided vs. Non-Voided RVEs

Table 7: A comparative summary of all four cases is presented in Table below, highlighting the influence of voids on mechanical properties.(FEM Abaqus CAE)

Loading Case	**Displacement**	**Non-Voided Strength**		**Voided Strength**		**Reduction (%)**	
	In (mm)	**E/modulus(Gpa)**	**Strength (MPa)**	**E/modulus(Gpa)**	**Strength(MPa)**	**E/modulus**	**Strength**
Density		1565.4		1533.36		2.046761211	
Tensile(Fiber Dir.)	0.2	146.3	29.3	144.65	28.9	1.12781	1.36518
Tensile (X-axis)	0.5	17.13	648	16.35	550	4.55341	15.1234
Compression (Y-axis)	-0.2	18	420	17.28	367.74	4	12.4428
Shear (XY-plane)	0.5	3.23	49.89	3.01	46.2	6.81114	7.396271

DISCUSSION

1. Density Reduction

The presence of voids led to a decrease in density from 1565.4 kg/m³ to 1533.36 kg/m³, indicating a material porosity increase and a decrease in density of 2.0%

2. Tensile Properties (Fiber Direction - Z-axis)

More pronounced reduction in modulus (146.3 MPa to 144.65 MPa) and strength (29.3 MPa to 28.9 MPa) making 1.1% and 1.3% respectvely, aligning with experimental trends where voids significantly impact longitudinal tensile strength .

3. Transverse Tensile (X-axis)

The modulus decreased from 17.13 MPa to 16.35 MPa, while strength significantly dropped from 648 MPa to 550 MPa, making 4.55% and 15.1% reduction respectively indicating a substantial void effect on transverse properties.

4. Compression (Y-axis)

More pronounced reductions, with modulus decreasing from 18 MPa to 17.28 MPa and strength dropping significantly from 420 MPa to 367.74 MPa marking 4% and 12.1% reduction respectively.

5. Shear (XT-plane)

Modulus reduced from 3.23 MPa to 3.01 MPa, with strength dropping from 49.89 MPa to 46.2 MPa marking 6.8% and 7.39% reduction respectively, showing a higher void effect in shear loading cases.

CONCLUSION

In conclusion, both analytical and FEM analyses clearly demonstrate that voids significantly reduce the mechanical performance of composite materials, with strength being more affected than elastic modulus. The most substantial reductions occur in matrix-dominated properties, particularly transverse tensile and shear strengths, which experienced drops of up to 15.12% and 7.39% respectively in FEM simulations. These findings highlight the heightened vulnerability of these properties to void-induced stress concentrations. The FEM approach proved especially effective in capturing localized damage mechanisms such as interfacial debonding and matrix cracking, making it more sensitive and accurate than analytical models in assessing the effects of voids. A strong correlation was also observed between void content and strength loss, consistent with existing literature—for instance, tensile strength decreased from 523 MPa to 415 MPa with increased void content. Notably, even a small void content of 2.66% led to up to 15% strength reduction in FEM results, emphasizing the critical impact of voids. In contrast, longitudinal properties showed minimal degradation (1–2%), reflecting the primary load-bearing role of the high-modulus fibers in that direction.

REFERENCES

[1] a. A. B. e. al, "Composite Materials for Aircraft Structures, Second Edition," October 2004.

[2] Z. Y. e. al, "Predicting the mechanical behaviour of highly particle-filled polymer composites using the nonlinear finite element method," *ELSEVIER*, 2022.

[3] P. Ferretti, "Representative Volume Element (RVE) Analysis for Mechanical Characterization of Fused Deposition Modeled Components," *Polymers*, 2021.

[4] Michael Okereke, "finite elements applications," *springer*.

[5] R. B. Heslehurst, "Defects and Damage in Composite Materials and Structures," *CRC Press.*

[6] Norkhairunnisa Mazlan, "Advanced Composites in Aerospace Engineering Applications," *Springer.*

[7] M. M. e. al, "Voids in fiber-reinforced polymer composites: A review on their formation, characteristics, and effects on mechanical performance, Journal of Composite Materials," p. 53, 2019.

[8] N. J. e. al, "Voids and their effects on mechanical-properties of omposites-appraisal," *sampe*, 1978.

[9] H. H. e. al, "Effects of void geometry on elastic properties of," 2005.

[10] J. K. e. al, "Void growth and resin transport during processing of thermosetting-matrix composites, Advanced in Polymer Science," *1986.*

[11] F. Campbell, "Porosity in carbon-fiber composites an over view of causes," *advanced materials*, 1995.

[11] R. O. e. al, "Effects of cure cycle pressure and voids on some mechanical properties of carbon/epoxy laminates, Composites," *2009.*

[12] A. L. e. al, "Curing of epoxy matrix composites," *composite materials.*

[13] S. L. e. al, "influence of cure pressure on microstructure, temperature field and mechanical properties of advanced polymer-matrix composite laminates," *fibers and polymeers*, 2014.

[14] X. Y. Yutong Fu, "A review on manufacturing defects and their detection of fiber reinforced resin matrix composites," *Composites*, 2022.

[15] F. C. et.al, "CE. Browning, Porosity in carbon-fiber composites An overview of causes, Journal of Advanced Materials," 1995.

[16] M. N. e. al, "Understanding the impact of fibre wrinkle architectures on composite laminates through tailored gaps and overlaps," *composires*, 2020.

[17] M. N. e. al, "Understanding the impact of fibre wrinkle architectures on composite laminates through tailored gaps and overlaps, Composites Part B," 2020.

[18] K. F. e. al, "Micro-level mechanisms of fiber waviness and wrinkling during hot drape forming of unidirectional prepreg composites, Composites: Part A," 2017.

[19] J. G. M. S. Ch. Jochum, "Proposal for a long-fibre microbuckling scenario during the cure of a thermosetting matrix," *Composites*, 2008.

[20] M. Å. Y.R. Larberg, "On the interply friction of different generations of carbon/epoxy prepreg systems," *Composites*, 2011.

[22] P. Hallander, "Forming induced wrinkling of composite laminates with mixed ply material properties; an experimental study, Composites: Part A," 2015.

[23] S. S, "Environmental effects on fibre reinforced polymericcomposites: evolving reasons and remarks on interfacial strength and stability. Adv Colloid Interface Sc".

[24] M. Piggott, "The effect of fibre waviness on the mechanical properties o unidirectional fibre composites: A review," *Composires Science and Technology.*

[25] R. S. S. M. S. H. N. Xie, "A numerical study on the influence of composite wrinkle defect geometry on compressive strength, Materials and Design," 2018.

[26] J. wood, "Void control for polymer-matrix composites," *composite manufacturing.*

[27] K. Y. e. al, "Experiment and analysis of mechanical properties of carbon fiber composite laminates under impact compression," *DE GRUYTER,* 2022.

[28] H. &. T. C. C. Hocheng, "The path towards delamination-free drilling of composite materials," *Journal of Materials Processing Technology.*

[29] R. S. D.A. Drake, "Prediction of delamination propagation in polymer," *Composites Part A,* 2019.

[30] H. R. R. I. M. P. S. S. M.J. Suriani, "Delamination and," *Delamination and* , 2021.

[31] E. N. M. Q. M. Z. P.A. Carraro, "Delamination onset in symmetric cross-ply laminates under static loads: Theory, numerics and experiments," *Composite Structures,* 2017.

[32] Y. L. Z. S. Z. L. J. C. X. L. X. J. D. Z. D. Geng, "Delamination formation, evaluation and suppression during drilling of composite laminates: A review," *Composite Structures,* 2019.

[33] C. C. F. W. C. Z. Z. Jia, "Analytical study of delamination damage and delamination-free drilling method of CFRP composite,," *Journal of Materials material processing,* 2020.

[34] R. S. B.D. Davidson, " Effect of finite width on deflection and energy release rate of an orthotropic double cantilever specimen,," *Journal of Composite Materials* .

[35] L. G. Z. L. K. H. T. Z. R. S. Ziheng Tang, "A comparative study of void characteristics on the mechanical response of UD composites," *Mechanics of Materials,* 2022.

[36] N. Judd, "Voids and their effects on mechanical-properties of omposites-appraisal, Sampe Journal," 1978.

[37] T. D. R. B. S. Erland, "Characterisation of inter-ply shear in uncured carbon fibre prepreg," *Composites,* 2015.

[38] S. Erland, "Characterisation of inter-ply shear in uncured carbon fibre prepreg, Composites: Part A," 2015.

[39] S. A. e. al, "Characterization and Effects of Fiber Pull-Outs in Hole Quality of Carbon Fiber Reinforced Plastics Composite," *MATERIALS,* 2016.

[40] F. A. e. al, "Cracks, microcracks and fracture in polymer structures: Formation,

detection, autonomic repair," *ELSEVIER , Progress in Materials Science,* 2016.

[41] a. K. Kaw, "mechanics of composite materials," 2006.

[42] H. e. al, "Size efects of voids on the mechanical properties of 3D printed parts," 2 May 2024.

[43] S. Zhang, "Effect of fabrication process on the microstructure and mechanical performance of carbon fiber reinforced PEEK composites via selective laser sintering," *Composites Science and Technology,* 2024.

[44] J. Z. e. al, "Influence of void defects on impact properties of CFRP laminates based on multi-scale simulation method," *ELSERVIER,* 2023.

[45] H. L. e. al, "The effect of voids on the quasi-static tensile properties of carbon fiber/polymer laminated composites," *composite materials* , 2017.

[46] y. L. e. al, "Study on the Efect of Void Defect on Mechanical Properties of carbon fiber composites by finite element method," 2022.

[47] L. H. &. L. P. Wenjun Bai, "Study of the effect of void defects on the mechanical properties of fiber reinforced composites," *Mechanics of Advanced Materials and Structures,* 2024.

[48] D. Roach, "Structural Health Monitoring for Aircraft: Viable Inspection Tool or Passing Fancy?," *FAA Airworthiness Assurance Center.*

[49] X. Qing, "Piezoelectric Transducer-Based Structural Health Monitoring for Aircraft Applications," 2019.

[50] E. J. Barbero, "Finite Element Analysis of Composite Materials," 2008.

[51] M. Kazemi and E. Fini, "State of the art in the application of functionalized waste polymers in the built environment," 2022.

[52] A. Rodrigues, F. Luís, V. Wandscher, G. Pereira, L. Valandro and M. J. P. Rippe, "Surface treatments of a glass fiber reinforced composite: Effect on the adhesion to acomposite resin," 2020.

[53] L. L. e. Al, "A Note on mori-tanaka's method," *AMSS Press,* 2014, june.

[54] ‡. C. B. M. N. R. S. Behrad Koohbor†, "Identification of RVE Length Scale in Fiber Composites via Combined Optical and SEM digital image correlation," 2022.

[55] Y. ·. V. Aanchna Sharma, "Representative volume element based micromechanical modelling of rod shaped glass flled epoxy composites," *springer,* 2021 january 28.

[56] M. Ostoja-Starzewski, "Material spatial randomness: From statistical to representative Volume element," *ELSEVIER,* 2006.